ATMOSPHERIC SCIENCE LETTERS
Atmos. Sci. Let. **16**: 119–126 (2015)
Published online 26 September 2014 in Wiley Online Library
(wileyonlinelibrary.com) **DOI:** 10.1002/asl2.532

RMetS
Royal Meteorological Society

The oscillation of the perturbation potential energy between the extratropics and tropics in boreal winter

Lei Wang,[1,2] Jianping Li,[3]* Zhanggui Wang,[2] Yanjie Li[4] and Fei Zheng[4]

[1]*School of Physics, Peking University, Beijing 100871, China*
[2]*Key Laboratory of Research on Marine Hazards Forecasting, National Marine Environmental Forecasting Center, Beijing 100081, China*
[3]*College of Global Change and Earth System Science, Beijing Normal University, 100875, China*
[4]*State Key Laboratory of Numerical Modeling for Atmospheric Sciences and Geophysical Fluid Dynamics, Institute of Atmospheric Physics, Chinese Academy of Sciences, Beijing 100029, China*

*Correspondence to:
J. Li, College of Global Change and Earth System Science, Beijing Normal University, Beijing 100875, China.
E-mail: ljp@bnu.edu.cn

Received: 9 January 2014
Revised: 3 July 2014
Accepted: 6 August 2014

Abstract

Correlation analyses reveal that the perturbation potential energy (PPE) in the extratropics and tropics in boreal winters undergoes out-of-phase oscillations (PPE1 extratropics–tropics oscillation, PETO). PETO is closely related to both El Niño-Southern Oscillation (ENSO) and kinetic energy, furthermore, PETO tends to dominate over the extratropics while ENSO is more important over the tropics. In the Northern (Southern) Hemisphere, positive PETO phases tend to strengthen (weaken) Hadley circulation and to weaken (strengthen) an expanded Ferrel circulation, resulting in equatorward shift of the subtropical jet streams. In addition, precipitation is enhanced in regions of ascending vertical motion, and warmer temperatures are observed in the tropics except over the western Pacific.

Keywords: perturbation potential energy; kinetic energy; oscillation; El Niño-Southern Oscillation; Hadley circulation; precipitation

1. Introduction

Energy is the driver of motion of the viscous atmosphere. Studies of the energy budget of the atmosphere can reveal the underlying causes of the formation and maintenance of atmospheric general circulation. If the atmosphere is taken as a heat engine, its efficiency is very low, with little potential energy available for conversion to kinetic energy (KE) (Peixoto and Oort, 1992). Therefore, the issue of the availability of atmospheric energy is vital, and has attracted much attention. Margules (1903) introduced the concept of available KE in storm studies, while the concept of available potential energy (APE) (Lorenz, 1955) was a milestone. Lorenz (1955) derived the formulation of APE and presented a view of global energy transformation that forms the basis of current atmospheric energetics. However, variations in atmospheric circulation exhibit strong regional features that cannot be explained by the theory of APE, which is based on global averages.

In order to study local energy efficiency, there has been much work on extending APE theory to the local scale (Oort, 1964; Smith, 1969a, 1969b; Johnson, 1970; Edmon, 1978; Gu, 1990; Hu *et al.*, 2004; Li *et al.*, 2007; Li *et al.*, 2011), however there are limitations. The definition of the reference state in APE theory is very important, but in previous studies it is empirical and dependent on the object of the study (Gao *et al.*, 2006; Gao and Li, 2007). It is also questionable whether a local-scale reference state is meaningful. Motivated by these limitations, Li and Gao (2006) proposed perturbation potential energy (PPE) to study local energy efficiency. PPE is based on a global reference state that is related to the atmospheric state before the adiabatic adjustment. PPE includes the contribution of the first-order perturbation, which vanishes in global averages and thus is not included in the APE. Note that the eddy energies developed by both Lorenz (1955) and Oort (1964) only consist of the global averaged temperature perturbations (APE), and do not include the contribution from the first-order term (PPE1).

PPE has a stronger relation to KE and atmospheric circulation on the regional scale than does APE (Gao and Li, 2012). Thus, PPE may be more relevant than APE to exploring the energy availability on a local scale. Wang *et al.* (2012) investigated the governing equations of PPE and KE that have been successfully applied to the South China Sea summer monsoon. The spatial structure of PPE is characterized by a zonal distribution (Li and Gao, 2006; Wang *et al.*, 2012; Wang *et al.*, 2013); analysis also reveals negative correlation of PPE1 between adjacent latitudes in January (Gao, 2006). We focus on the PPE1 extratropics–tropics oscillation (PETO) in boreal winters. Given the importance of energy budgets for atmospheric general circulation, the way in which the PETO may act to change the atmospheric general circulation is of great scientific interest.

The El Niño-Southern Oscillation (ENSO) is well known as the dominant mode of interannual variability in the tropical climate and has profound effects on the global climate system. Goddard and Philander (2000) documented the energetics of interannual variability of ENSO from a realistic ocean model. On the basis of two reanalysis datasets, Li *et al.* (2011) showed that the

increase in global mechanical energy in El Niño years is due to changed atmospheric temperature gradients driven by a tropical sea surface temperature (SST) anomaly. Examination of the relation between PPE and ENSO is desirable, and may help us understand the influence of ENSO on the general circulation. This work explores the relationship between ENSO, KE, and PETO, and then investigates the physical meaning and climate impact of PETO.

2. Data and methodology

This study employs temperature, wind, specific humidity, surface pressure, 2 m air temperature, and 10 m horizontal wind from two atmospheric reanalysis datasets: the NCEP–DOE Reanalysis 2 (Kanamitsu *et al.*, 2002) and the European Centre for Medium-Range Weather Forecast (ECMWF) reanalysis dataset (ERA-Interim) (Dee *et al.*, 2011). We use two rainfall analysis datasets: the Climate Prediction Center (CPC) Merged Analysis of Precipitation (CMAP) (Xie and Arkin, 1997) and the Global Precipitation Climatology Project (GPCP) (Adler *et al.*, 2003). Note that the NCEP 2 and CMAP have been used in the following analysis, and the ERA-Interim and GPCP used for validation. Global SST is obtained from the Extended Reconstructed Sea Surface Temperature (ERSST.v3) on a $2^\circ \times 2^\circ$ grid (Smith *et al.*, 2008). ENSO is quantified by the Niño3.4 index, which is defined as the areal mean sea surface temperature anomaly (SSTA) over the region 5°S–5°N, 170°–120°W. The analysis is based on boreal winters (December to February; DJF) for the period 1979–2013.

The mathematical expression of PPE (Li and Gao, 2006) is:

$$P'_{\mathrm{Li}} = \frac{p_{00}^{(i-1)\kappa}\prod_{j=0}^{i-1}(1+\kappa-j)}{i!r_{\mathrm{d}}(1+\kappa)}\int_0^{p_{\mathrm{s}}}\frac{T'^i}{p^{(i-1)(1+\kappa)}} \times\left(-\frac{\partial\overline{\theta}}{\partial p}\right)^{-i+1}dp \quad (1)$$

where i is the order of PPE, p_{00} is reference pressure (usually taken as 1000 hPa), and p_{s} is surface pressure. Here also $\kappa = R/c_{\mathrm{p}}$, where R is the gas constant of dry air, c_{p} is specific heat at constant pressure, while $r_{\mathrm{d}} = g/c_{\mathrm{p}}$ is the dry adiabatic lapse rate, with g the gravitational acceleration; p is pressure, T is temperature, and θ is potential temperature. Additionally $\overline{T}$ represents a global average on an isobaric surface and T' the departure from this global average. The formulas for first-order PPE (PPE1) and second-order PPE (PPE2) can be expressed as:

$$\mathrm{PPE1} = \frac{1}{r_{\mathrm{d}}}\int_0^{p_{\mathrm{s}}} T'dp \quad (2)$$

$$\mathrm{PPE2} = \frac{\kappa p_{00}^{\kappa}}{2r_{\mathrm{d}}}\int_0^{p_{\mathrm{s}}}\frac{T'^2}{p^{1+\kappa}}\left(-\frac{\partial\overline{\theta}}{\partial p}\right)^{-1}dp \quad (3)$$

It can be seen that the global average of PPE2 equals the APE (when higher orders of $p'/\overline{p}$ are neglected). Li and Gao (2006) have examined the distribution and magnitude of PPE1 and PPE2. Locally, PPE1 is an order of magnitude larger than PPE2. Hence, we focus on PPE1.

The governing equations of PPE1 and KE (Wang *et al.*, 2012) are:

$$\frac{\partial}{\partial t}\mathrm{PPE1} = \mathfrak{T}_L + \aleph_L + R_L - C_K + G_L \quad (4)$$

$$\frac{\partial}{\partial t}\mathrm{KE} = B_K + \mathfrak{R}_K + C_K + M_K \quad (5)$$

Here $\mathrm{KE} = g^{-1}\int_0^{p_{\mathrm{s}}} e_k dp$; $C_K = g^{-1}\int_0^{p_{\mathrm{s}}}\omega\left(\partial\phi'/\partial p\right)dp$ is a conversion term between PPE1 and KE, which depends on vertical velocity and atmospheric stability; $G_L = g^{-1}\int_0^{p_{\mathrm{s}}} Q'dp$ is the source (sink) term of PPE1, which depends on nonuniform diabatic heating; $M_K = g^{-1}\int_0^{p_{\mathrm{s}}}\overrightarrow{V_h}\overrightarrow{\Upsilon_h}dp$ is viscous dissipation, with $\overrightarrow{V_h}$ the horizontal velocity vector and $\overrightarrow{\Upsilon_h}$ the horizontal friction force; $\mathfrak{T}_L$ and B_K are horizontal boundary terms; and $\aleph_L$, R_L, and $\mathfrak{R}_K$ are topographically induced terms. More details on the derivation of PPE and related governing equations are given in the Supporting Information.

3. Results

3.1. PPE extratropics–tropics oscillation

Figure 1(a) shows the cross correlations between zonally averaged PPE1 anomalies in DJF. The most prominent features are the significant negative correlations between PPE1 at the tropics and extratropics in both hemispheres. The correlation coefficient between $\langle\mathrm{PPE1}\rangle_{10^\circ\mathrm{S}}$ and $\langle\mathrm{PPE1}\rangle_{45^\circ\mathrm{S}}$ is −0.78, between $\langle\mathrm{PPE1}\rangle_{10^\circ\mathrm{S}}$ and $\langle\mathrm{PPE1}\rangle_{32.5^\circ\mathrm{N}}$ −0.51, and between $\langle\mathrm{PPE1}\rangle_{45^\circ\mathrm{S}}$ and $\langle\mathrm{PPE1}\rangle_{32.5^\circ\mathrm{N}}$ 0.57, all above the 99% confidence level. These results suggest an out-of-phase pattern in PPE1 anomalies between the extratropics and tropics, and in-phase relations within the extratropics and tropics. The tripole-like PPE1 variations represent the oscillation in PPE on a global scale. When PPE1 in the tropics is enhanced, that in the extratropics tends to be suppressed, and thus, this oscillation is referred to as the PPE extratropics–tropics oscillation. To further examine the interannual variation of PETO, a PPE1 extratropics–tropics oscillation index (PETOI) is defined as the difference in the normalized zonally averaged PPE1 between the tropics and extratropics:

$$\mathrm{PETOI} = \left(\langle\mathrm{PPE1}\rangle_{10^\circ\mathrm{S}} + \langle\mathrm{PPE1}\rangle_{10^\circ\mathrm{N}} - \langle\mathrm{PPE1}\rangle_{32.5^\circ\mathrm{N}} - \langle\mathrm{PPE1}\rangle_{45^\circ\mathrm{S}}\right)/2$$

These are the latitudes at which the extrema of correlations between PPE1 over the tropics and extratropics occur. Henceforth, we define positive (negative) PETO winters as winters with a PETOI value >1 (<−1) standard deviation of the index. The positive PETO phase

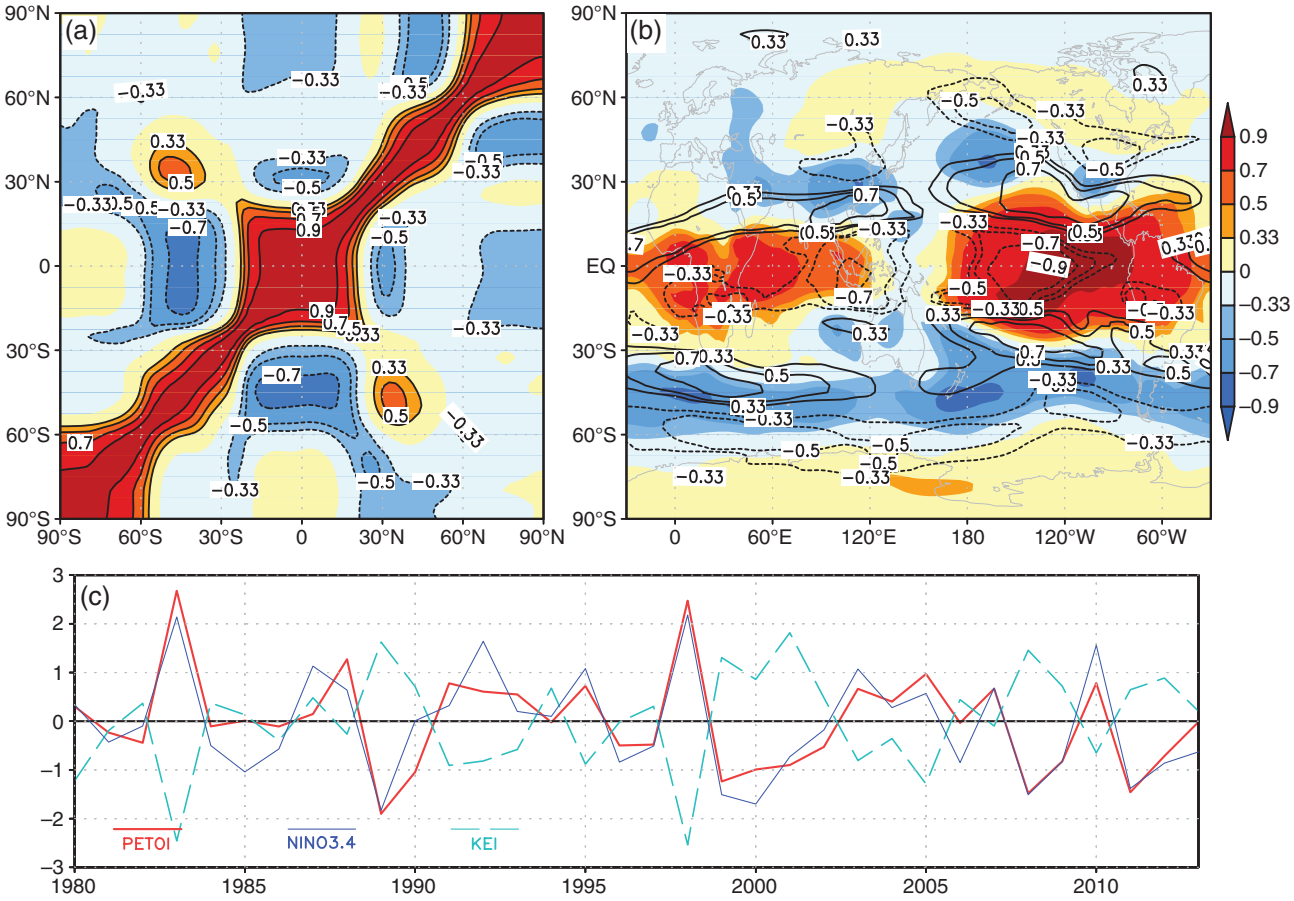

Figure 1. (a) Cross correlations between zonally averaged PPE1 anomalies in DJF; (b) correlation maps between PETOI and PPE1 (shading), and KE (contours) in DJF; (c) normalized time series of PETOI, Niño3.4, and KEI.

is characterized by enhanced PPE1 in the tropics and suppressed PPE1 in the extratropics. Conditions are reversed in the negative phase.

To explore the spatial pattern of the PETO, the correlation map of PETOI with PPE1 is shown in Figure 1(b). The tropics (excluding the western Pacific) are dominated by significant positive correlations, accompanied by significant negative correlations in the central North Pacific, subtropical Asia and North America, and over 30°–60°S, which indicates that the PETOI is capable of describing the PETO.

3.2. Importance of the PETO in the relationship between ENSO and KE

Figure 1(b) also shows correlations between PETOI and KE. Negative correlations dominate the tropics and positive correlations dominate the subtropics. The pattern is nearly opposite to that of PETO, indicating the close relationship between PPE and KE. To further investigate the relations between PETOI and KE, the KE index (KEI) is defined as the difference in the normalized zonally averaged KE:

$$\mathrm{KEI} = \left(\langle \mathrm{KE}\rangle_{10°\mathrm{S}} + \langle \mathrm{KE}\rangle_{0°} - \langle \mathrm{KE}\rangle_{22.5°\mathrm{N}} - \langle \mathrm{KE}\rangle_{32.5°\mathrm{S}}\right)/2$$

These latitudes are chosen as they represent the extrema of correlations between PPE1 and KE. Figure 1(c) shows normalized time series of the PETOI, KEI, and Niño3.4 index. Extremes of positive PETOI (negative KEI) occurred in the winters of 1982/1983 and 1997/1998 when a strong El Niño occurred, while negative PETOI (positive KEI) extremes occurred in the winters of 1988/1989 and 1998/1999 when there was a strong La Niña. Notably, Niño3.4 correlates positively with PETOI with a value of 0.88. This indicates that the interannual variability in PETO is closely related to ENSO. On the other hand, KEI varies inversely with PETOI and the correlation coefficient between them is −0.91. Figure 2(b) shows that the correlation is also significant when PETOI precedes KEI. It is speculated that the energy conversion between PPE1 and KE may be responsible for the inverse correlation.

Figure 2(a) illustrates correlation coefficients between the winter PETOI and previous autumn SSTA. It is clear that when SSTA leads PETOI by 3 months, the mid-eastern tropical Pacific SSTA is positively correlated with PETOI, and the correlation pattern resembles a clear ENSO signal. The simultaneous correlation patterns (Figure 2(c)) are quantitatively similar to the corresponding lead–lag counterparts (Figure 2(a)); the simultaneous correlation patterns are also consistent with previous studies (Gao and Li,

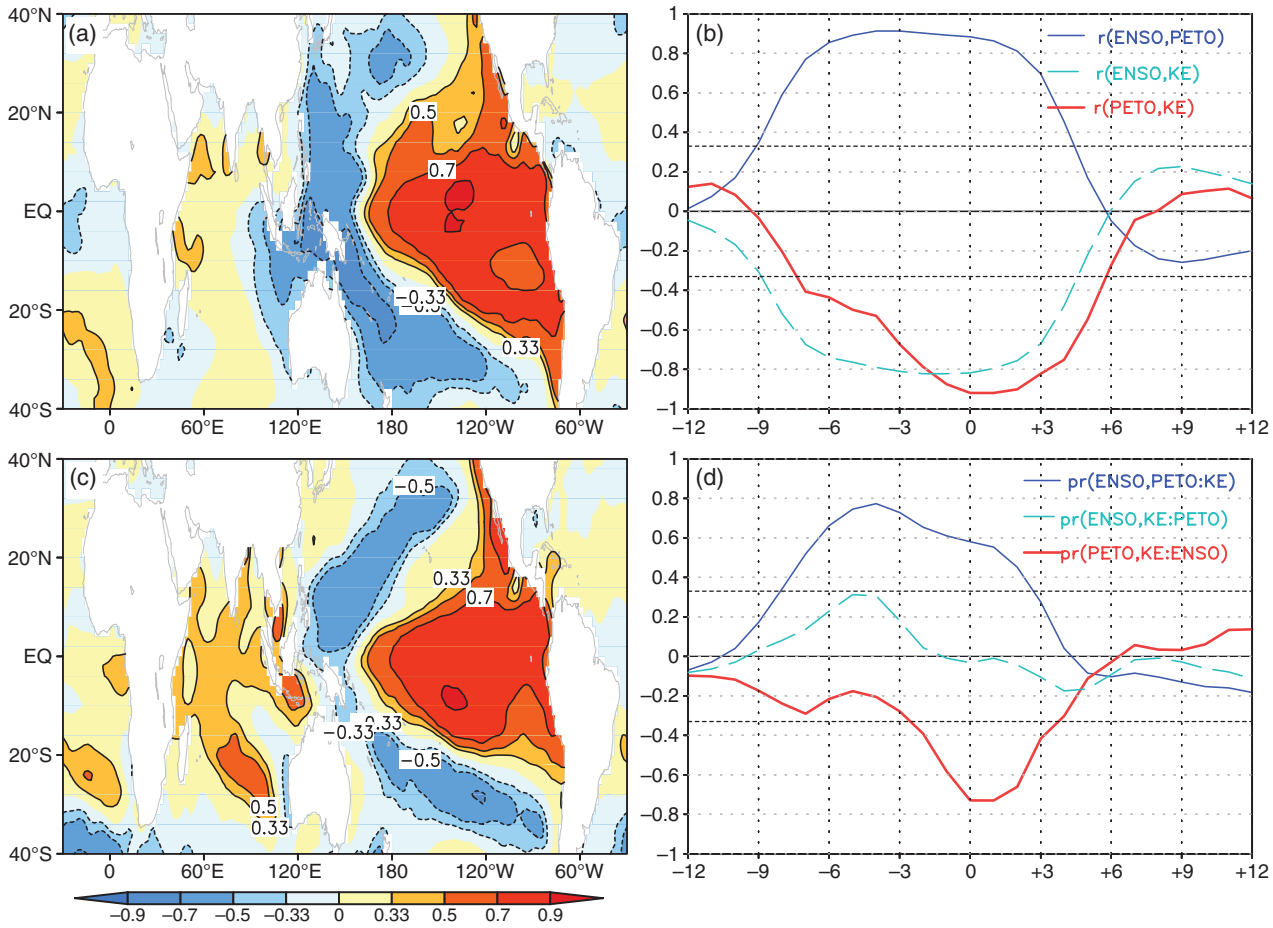

Figure 2. Correlation coefficients between the PETOI (DJF) and SSTA in (a) previous boreal autumn (SON), (c) simultaneous DJF, (b) lead–lag correlations between Niño3.4 and PETOI, Niño3.4 and KEI, PETOI and KEI for different months, (d) the same as (b) but for partial correlations. The correlation between X and Y is written as $r(X, Y)$, while the partial correlation between X and Y adjusted for variable Z is written as $\mathrm{pr}(X, Y: Z)$.

2013). Furthermore, Figure 2(b) shows that a robust leading correlation between Niño3.4 and PETOI develops the previous spring, peaks the previous autumn and persists for the following 6 months until it decays.

To further study the relationships between PETO, ENSO, and KE, partial correlations are also performed. As shown in Figure 2(d), the connection between ENSO and PPE1 is not affected by removing the effect of KE, which suggests that ENSO has a significant control on PPE1. In contrast, the partial correlations between Niño3.4 and KEI change drastically when the effect of the PETOI is removed: the leading signal shows a reversal in sign and becomes insignificant. This may indicate that PPE1 plays a major role in the influence of ENSO on KE. Notably, the partial correlations between PETOI and KEI adjusted for Niño3.4 change little: the leading signal is still significant in the previous autumn, and peaks in winter. These results suggest that the physical linkage between PPE1 and KE is more direct than that between ENSO and KE. The connection between PPE1 and ENSO results from the related heating anomaly that contributes to the source/sink of PPE1. These results suggest that the interannual variation of PPE is modulated by ENSO, and that the PPE can then affect KE through energy adjustment.

3.3. Anomalous circulation associated with PETO

When energy changes between different forms the atmospheric circulation becomes disturbed. Here we examine the atmospheric circulation pattern associated with PETO. Figure 3(a)–(d) shows maps of the correlation between the PETOI and related variables. A few key characteristics associated with positive PETOI winters are listed below.

We reported the strong relation between PETO and KE in the previous section. Figure 3(a) further shows that positive (negative) KE anomalies develop over the equatorward (poleward) section of the subtropical jet streams, and negative KE anomalies occupy the tropical easterlies belt, generally opposite to the variations of PPE1. Figure 3(b) shows that anomalous westerlies (easterlies) are situated over the equatorward (poleward) section of the subtropical jet streams. This results in a shift of the subtropical jet streams toward the equator, which further influences the extratropical storms and frontal systems. Figure 3(c) shows that, in the Northern Hemisphere, the anomalous direct circulation loop (DCL) situated in the tropics results in a strengthened Hadley circulation (HC), while the DCL situated in middle latitudes weakens the Ferrel circulation (FC).

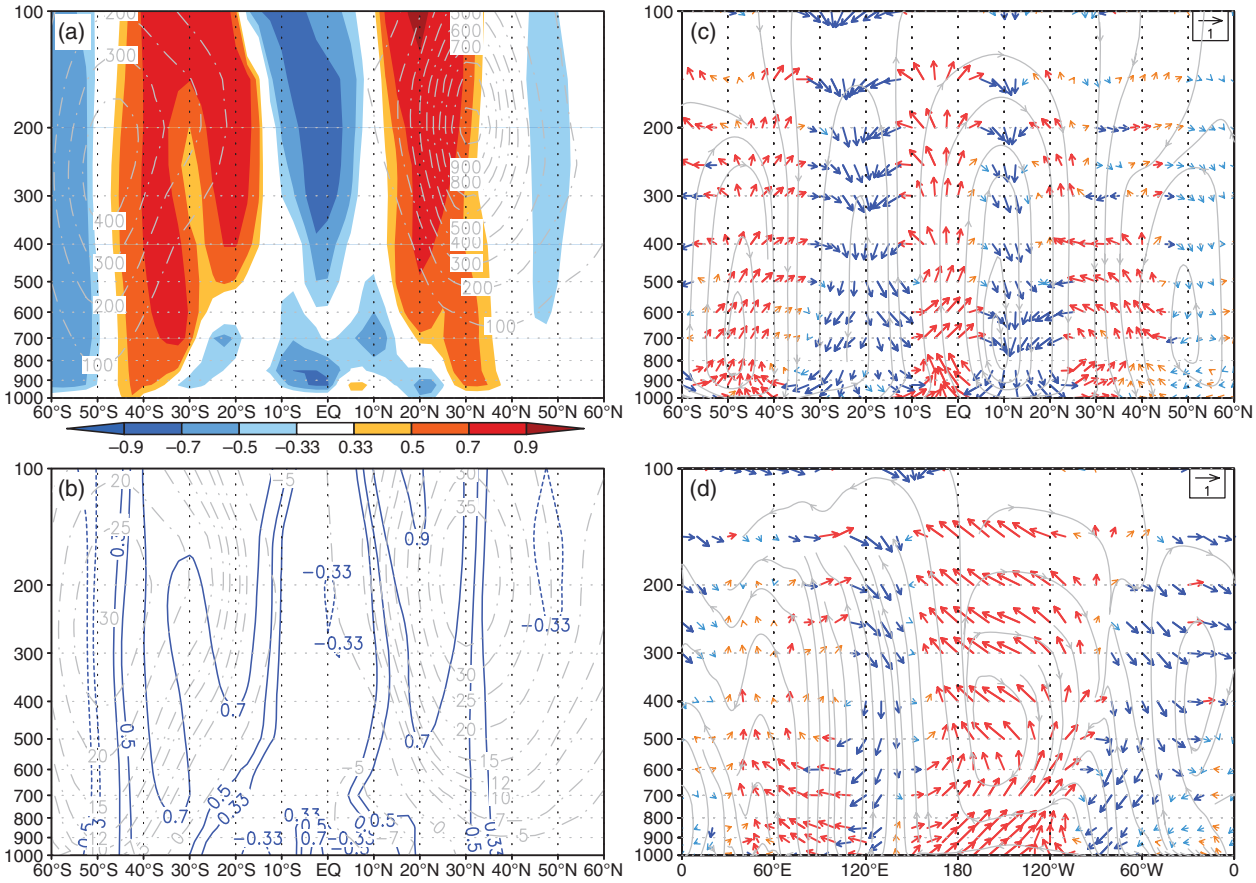

Figure 3. Correlation coefficients between PETOI and (a) zonally averaged KE (shading), (b) zonally averaged zonal wind (blue lines), (c) zonally averaged meridional circulation (red vectors), and (d) zonal circulation averaged over 5°S–5°N. Climatological (1980–2013) zonally averaged (a) KE (grey dashed line, units: J kg^{-1}); (b) u-wind (grey dashed line, units: m s^{-1}); and (c) meridional circulation (grey streamline, units of horizontal and vertical components are m s^{-1} and -10^{-2} Pa s^{-1}, respectively). Shading in (a) and red/blue vectors in (c), (d) indicate significance at the 95% confidence level. Orange/light blue vectors are used for lower confidence levels.

The anomalous indirect circulation loop (ICL) induces shrinking of the HC and expansion of the FC, so that the subtropical jet stream moves toward the equator. In the Southern Hemisphere, the combined anomalous DCL and ICL cause the FC to strengthen and expand toward the equator. Figure 3(d) shows the correlation between PETO and meridionally averaged (5°S–5°N) zonal velocity and vertical velocity. The most important feature in the anomalous Walker circulation is the ascent in the central–eastern tropical Pacific and descent in the western tropical Pacific in positive PETOI years. Regions of anomalous vertical motion may experience a build-up of deep convection and heavy rainfall.

To clarify the impact of PETO and ENSO on atmospheric circulation, Figure 4(a) and (b) shows the partial correlation between PETOI and related zonally averaged variables after removing the effect of ENSO. In the positive phase of PETOI, the distribution of KE (Figure 4(a)) features positive anomalies over the equatorial section of the subtropical jet. In addition, the zonal wind pattern (Figure 4(b)) still captures the anomalous westerlies over the subtropics. Figure 4(c) and (d) shows the partial correlation between ENSO and related zonally averaged variables after removing the effect of the PETOI. In El Niño years, the negative KE anomalies over the tropics (Figure 4(c)) bear some similarity to the correlation between ENSO and KE. In contrast, anomalous westerlies (Figure 4(d)) occur over the tropics. These results indicate that ENSO tends to dominate over the tropics while the PETO is more important over the extratropics.

3.4. Impact of PETO on climate

It is expected that the large-scale circulation anomalies corresponding to PETO may have considerable impact on climate. Figure 5(a) and (b) depicts the correlation between the PETOI and precipitation and surface temperature, respectively.

As shown in Figure 5(a), the winter PETOI is positively correlated with precipitation in the central–eastern tropical Pacific, whereas it is negatively correlated with precipitation over the Maritime Continent. Thus when the winter PETOI is positive, the central–eastern tropical Pacific experiences wetter conditions in contrast to the drier conditions in the Maritime Continent. In addition, significant positive correlation develops in and to the east of southeast China, in subtropical North America and over the Atlantic Ocean, suggesting wetter conditions over

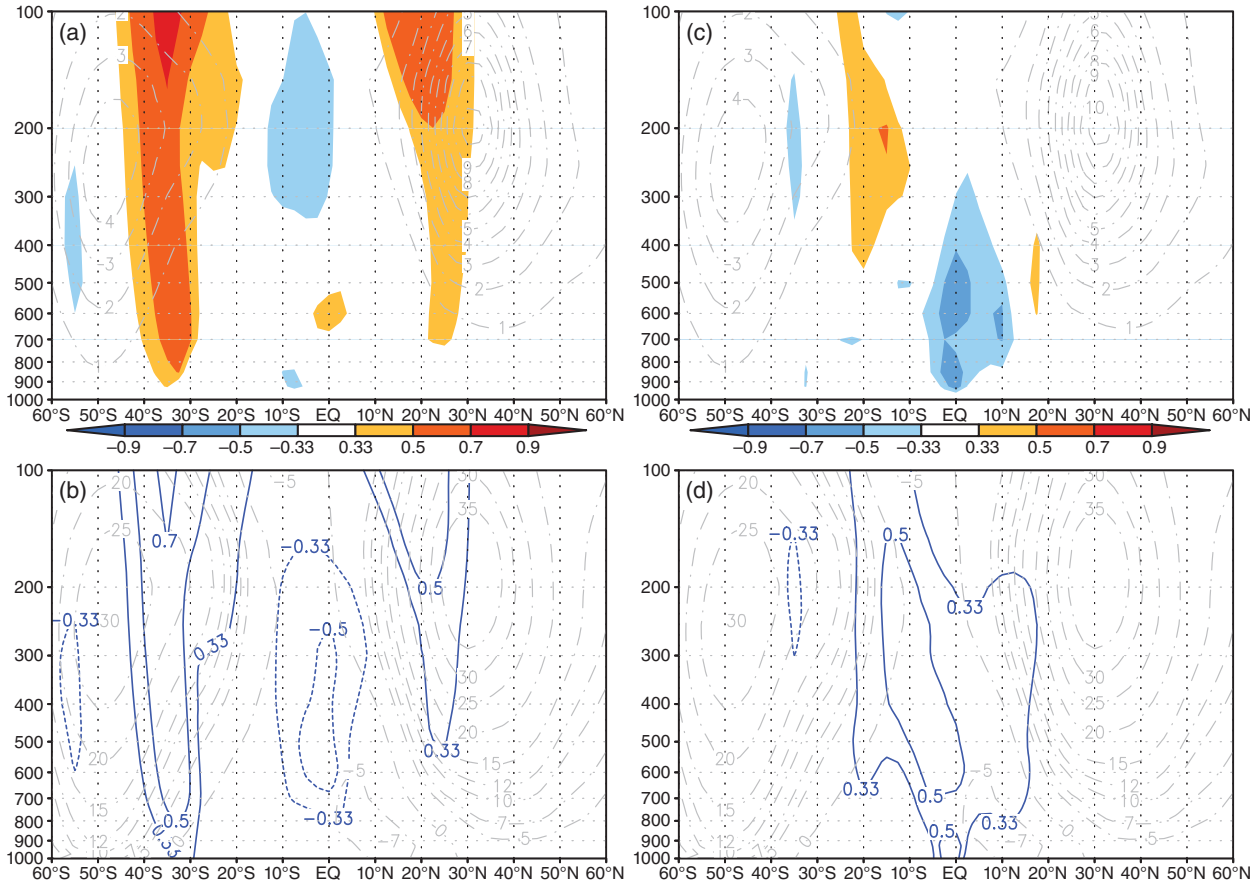

Figure 4. Partial correlation between PETOI and zonally averaged (a) KE (shading), (b) zonal wind (blue line) with the effect of ENSO removed. Partial correlation between ENSO and zonal-averaged (c) KE (shading), (d) zonal wind (blue line) with the effect of PETOI removed. Climatology is shown as in Figure 3.

these regions in a positive PETOI phase. In contrast, significant negative correlations are observed in equatorial South America, southwestern Australia, and southern Africa, indicating drier conditions in these regions associated with a positive PETOI. As precipitation is directly associated with moisture transport, it is useful to investigate possible connections between the PETO and moisture transport. The results suggest strong convergence accompanies the abundant rainfall. Figure 5(b) shows that significant positive correlation between the winter PETOI and surface air temperature (SAT) occurs in western North America and the tropics except in the western Pacific, indicating above-normal temperature conditions in these regions in positive PETOI years. The correlation pattern between PETOI and temperature advection suggests that anomalous warming is usually related to warm advection (currents) originating from low latitudes (the warm ocean).

To further clarify the influence of PETO on climate, we employ partial correlations to exclude the possible effects of Niño3.4. Figure 5(c) shows positive correlation in the eastern tropical Pacific, but negative correlation over the central tropical Pacific and North China Plain, indicating that more rainfall develops in the eastern tropical Pacific, but less rainfall in the central tropical Pacific and North China Plain in positive phases of PETOI. Figure 5(d) shows significant negative correlation between SAT and PETOI in eastern China, indicating cooling in eastern China in positive PETOI years.

The effects of ENSO on global patterns of abnormal rainfall and SAT have been extensively discussed (Ropelewski and Halpert, 1987; Halpert and Ropelewski, 1992). We also examine partial correlations between ENSO and related variables to exclude the possible effects of PETOI. Figure 5(e) shows positive correlation over the equatorial central Pacific, tropical North America and North China Plain, implying that rainfall tends to be greater than normal in these regions in El Niño years. Moreover, the Niño3.4 index correlates negatively with rainfall over the tropical western Pacific and tropical South America, implying that these regions becomes drier than normal in El Niño years. Figure 5(f) shows that positive correlation appears in eastern China, suggesting that warming dominates eastern China in El Niño years.

4. Summary and discussion

On the basis of the PPE theory, PETO is identified in boreal winter using a statistical method. With positive (negative) PETO, PPE1 is enhanced (suppressed) in the tropics and suppressed (enhanced) in the extratropics.

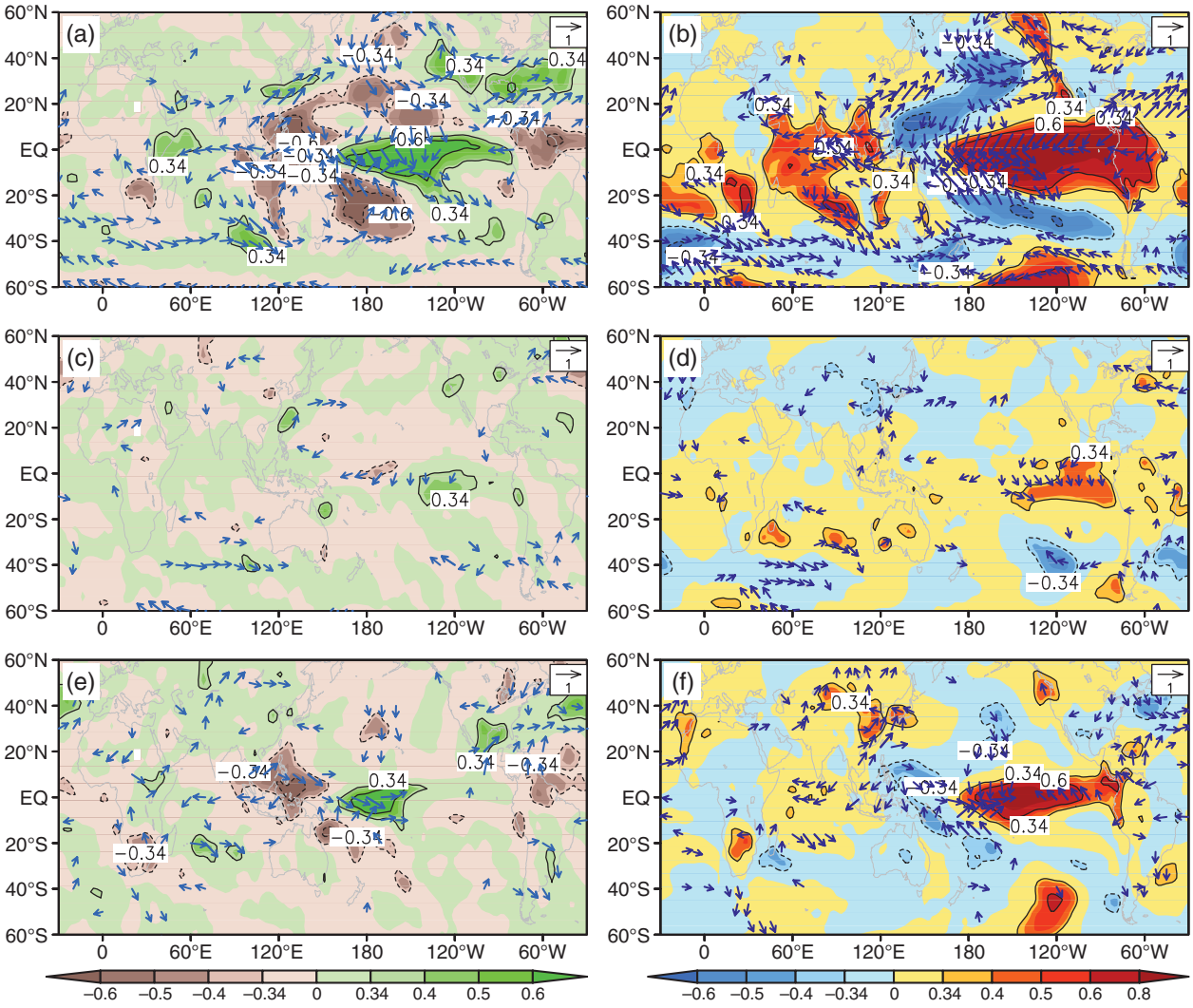

Figure 5. Correlation coefficients between the PETOI and (a) vertically integrated moisture transport (vectors) and precipitation (shading), (b) 10 m horizontal wind (vectors) and 2 m temperature (shading) in DJF (1980–2010); (c, d) same as (a, b) but for partial correlations with the effect of Niño3.4 removed; (e, f) same as (a, b) but for partial correlations between Niño3.4 and anomalies with the effect of PETOI removed. Vectors that are significant at the 95% confidence level are shown.

The PETO is significantly positively correlated with ENSO and negatively correlated with KE. These correlations persist for both simultaneous and lead–lag relationships. The composite difference of generation terms of PPE1 in El Niño and La Niña years (not shown) indicates that sources of PPE1 are observed near the equator whereas sinks of PPE1 are observed in the tropics away from the equator, supporting the physical linkage between the ENSO and PPE1. With positive (negative) PETO, KE is suppressed (enhanced) over the tropics and enhanced (suppressed) over the subtropics. Theoretically, the relation between PPE1 and KE is linked by a conversion term, which may be responsible for the significant correlation. These results suggest that PETO may be the key linkage between heating anomalies and KE perturbations.

A negative (positive) PETO phase is associated with weakened (strengthened) HC and shrinking–strengthened (expanding–weakened) FC in the Northern Hemisphere, with strengthened (weakened) HC and shrinking–weakened (expanding–strengthened) FC in the Southern Hemisphere, which favors poleward (equatorward) shift of the subtropical jet stream. Moreover, the partial correlation analysis indicates that ENSO tends to dominate over the tropics while PETO is more important over the extratropics.

The precipitation anomalies associated with PETO emerge as a result of the combined effects of anomalous descent (ascent) and moisture divergence (convergence). Warm anomalies appear in the tropics apart from the western Pacific in positive PETOI years, and may be attributed to warm advection.

The above results were validated by comparison with those found from data obtained from the ERA-Interim and precipitation data from the GPCP. Generally, the results are independent of the data source. While the this article reports the PETO and the relations between ENSO, KE and anomalous circulation patterns based on statistical analysis, further studies are required to investigate the detailed mechanisms of the underlying interactions.

Acknowledgements

We thank the editor Dr Christopher Holloway and two anonymous reviewers for their valuable comments which greatly improve our manuscript. This work is jointly supported by the National Basic Research Program of China (Grant No. 2010CB950400 and 2010CB950303), and the National Natural Science Foundation of China (Grant No. 41205034).

Supporting information

The following supporting information is available:

Appendix S1. The derivation of perturbation potential energy and its governing equations.

Figure S1. Global distribution of area-weighted PPE1 (left panels, units: $10^6\,\mathrm{Jm}^{-2}$), and PPE2 (right panels, units: $10^6\,\mathrm{Jm}^{-2}$). Annual means (top panels), winter (middle panels; DJF), and summer (lower panels; JJA).

Figure S2. Global distribution of area-weighted column-integrated generation term (GEN) of PPE1 (left panels, units: Wm^{-2}), and conversion term (CON) from PPE1 to KE (right panels, units: Wm^{-2}). Annual means (top panels), winter (middle panels; DJF), and summer (lower panels; JJA).

References

Adler RF, Huffman GJ, Chang A, Ferraro R, Xie P, Janowiak J, Rudolf B, Schneider U, Curtis S, Bolvin D, Gruber A, Susskind J, Arkin P. 2003. The version 2 Global Precipitation Climatology Project (GPCP) monthly precipitation analysis (1979-present). *Journal of Hydrometeorology* **4**: 1147–1167.

Dee DP, Uppala SM, Simmons AJ, Berrisford P, Poli P, Kobayashi S, Andrae U, Balmaseda MA, Balsamo G, Bauer P, Bechtold P, Beljaars ACM, van de Berg L, Bidlot J, Bormann N, Delsol C, Dragani L, Fuentes M, Geer AJ, Haimberger L, Healy SB, Hersbach H, Hólm EV, Isaksen L, Kållberg P, Köhler M, Matricardi M, McNally AP, Monge-Sanz BM, Morcrette JJ, Park BK, Peubey C, de Rosnay P, Tavolato C, Thépaut JN, Vitart F. 2011. The ERA-interim reanalysis: configuration and performance of the data assimilation system. *Quarterly Journal of the Royal Meteorological Society* **137**(656): 553–597.

Edmon HJ. 1978. A reexamination of limited area available potential energy budget equations. *Journal of the Atmospheric Sciences* **35**(9): 1655–1659.

Gao L. 2006. *Theoretical Studies and Diagnostic Analyses of Perturbation Potential Energy*. PhD dissertation, Institute of Atmospheric Physics, Chinese Academy of Sciences: Beijing; 1–33 (in Chinese).

Gao L, Li JP. 2007. Progress in the study of atmospheric energy efficiency. *Advances in Earth Science* **22**(5): 486–494.

Gao L, Li JP. 2012. Relationship and mechanism between perturbation potential energy and atmospheric general circulation anomalies. *Chinese Journal of Geophysics* **55**(3): 359–374.

Gao L, Li JP. 2013. Impacts and mechanism of diabatic heating on atmospheric perturbation potential energy. *Chinese Journal of Geophysics* **56**(10): 3255–3269.

Gao L, Li JP, Ren HL. 2006. Some characteristics of the atmosphere during an adiabatic process. *Progress in Natural Science* **16**(6): 644–648 (in Chinese).

Goddard L, Philander SG. 2000. The energetics of El Niño and La Niña. *Journal of Climate* **13**: 1496–1516.

Gu XZ. 1990. A theoretical study of the available potential energy in a limited atmospheric region. *Acta Meteorologica Sinica* **48**(2): 248–252 (in Chinese).

Halpert MS, Ropelewski CF. 1992. Surface temperature patterns associated with the Southern Oscillation. *Journal of Climate* **5**: 577–593.

Hu Q, Tawaye Y, Feng S. 2004. Variations of the Northern Hemisphere atmospheric energetics: 1948–2000. *Journal of Climate* **17**: 1975–1986.

Johnson DR. 1970. The available potential energy of storms. *Journal of the Atmospheric Sciences* **27**(5): 727–741.

Kanamitsu M, Ebisuzaki W, Woollen J, Yang SK, Hnilo JJ, Fiorino M, Potter GL. 2002. NCEP-DEO AMIP-II Reanalysis (R-2). *Bulletin of the American Meteorological Society* **83**: 1631–1643.

Li JP, Gao L. 2006. Theory on perturbation potential energy and its applications – concept, expression and spatiotemporal structures of PPE. *Chinese Journal of Atmospheric Sciences* **30**(5): 834–848.

Li L, Ingersoll AP, Jiang X, Feldman D, Yung YL. 2007. Lorenz energy cycle of the global atmosphere based on reanalysis datasets. *Geophysical Research Letters* **34**: L16813, doi: 10.1029/2007GL029985.

Li L, Jiang X, Chahine MT, Wang JQ, Yung YL. 2011. The mechanical energies of the global atmosphere in El Niño and La Niña years. *Journal of Atmospheric Sciences* **68**: 3072–3078.

Lorenz EN. 1955. Available potential energy and the maintenance of the general circulation. *Tellus* **7**(2): 157–167.

Margules M. 1903. *Über die Energie der stürme. Jahrbuch*. Zentralanstalt für. Meteorologie und Geodynamik: Wien; 1–26.

Oort AH. 1964. On estimate of the atmospheric energy cycle. *Monthly Weather Review* **92**: 483–493.

Peixoto JP, Oort AH. 1992. Chapter 14. *Physics of Climate*. American Institute of Physics Press: New York, NY.

Ropelewski CF, Halpert MS. 1987. Global and regional scale precipitation patterns associated with the El Niño/Southern Oscillation. *Monthly Weather Review* **115**(8): 1606–1626.

Smith PJ. 1969a. A computational study of the energetics of a limited region of the atmosphere. *Tellus* **21**(2): 193–201.

Smith PJ. 1969b. On the contribution of a limited region to the global energy budget. *Tellus* **21**(2): 202–207.

Smith TM, Reynolds RW, Peterson TC, Lawrimore J. 2008. Improvements to NOAA's historical merged land-ocean surface temperature analysis (1880-2006). *Journal of Climate* **21**: 2283–2296.

Wang L, Li JP, Guo Y. 2012. Governing equations of atmospheric layer perturbation potential energy and its applications – energy budget of the South China Sea summer monsoon activity. *Chinese Journal of Atmospheric Sciences* **36**(4): 769–783.

Wang L, Li JP, Ding RQ. 2013. Theory on layer perturbation potential energy and its applications – cases study on annual variation of the South China Sea summer monsoon. *Chinese Journal of Geophysics* **56**(2): 392–408 (in Chinese).

Xie PP, Arkin PA. 1997. Global precipitation: a 17-year monthly analysis based on gauge observations, satellite estimates, and numerical model outputs. *Bulletin of the American Meteorological Society* **78**: 2539–2558.

